Electronic Supplementary Material (ESI) for ChemComm.
This journal is © The Royal Society of Chemistry 2014

Electronic Supplementary Information

Ion-based assemblies of planar anion complexes and cationic Pt^{II} complexes

Ryo Sekiya, Yusuke Tsutsui, Wookjin Choi, Tsuneaki Sakurai, Shu Seki,* Yuya Bando and Hiromitsu Maeda*

College of Pharmaceutical Sciences, Ritsumeikan University, Kusatsu 525–8577, Japan, Fax: +81 77 561 2659; Tel: +81 77 561 5969; E-mail: maedahir@ph.ritsumei.ac.jp and Department of Applied Chemistry, Graduate School of Engineering, Osaka University, Suita 565–0871, Japan

Table of Contents

1. Preparation of Pt complexes and ion pairs

General procedures. Starting materials were purchased from Wako Pure Chemical Industries Ltd., TCI Chemical Co., and Sigma-Aldrich Co., which were used without further purification. BF_2 complexes of 1,3-di(5-phenylpyrrol-2-yl)-1,3-propanedione (**1a**),[S1] 1,3-bis(5-(3,4,5-trihexadecyloxyphenyl)pyrrol-2-yl)-1,3-propanedione (**1b**),[S2] and 1,3-bis(5-(3,4,5-trimethoxyphenyl)pyrrol-2-yl)-1,3-propanedione (**1b′**)[S2] were synthesized according to the literature procedures. ^{1}H and ^{19}F NMR spectra were recorded on a JEOL ECA-600 600 MHz spectrometer and were referenced to solvent (^{1}H) and hexafluorobenzene (^{19}F) at δ = −164.9 ppm. Matrix-assisted laser desorption ionization time-of-flight mass spectrometries (MALDI-TOF-MS) were recorded on a Shimadzu Axima-CFR plus using positive ion modes. Elemental analyses were performed on a Yanaco CHN corder MT series for carbon, hydrogen, and nitrogen and the oxygen flask combustion method and the subsequent potentiometric titration of silver using sodium ion selective glass electrode, wherein the data was recorded on a Hiranuma Sangyo Co. Ltd. auto titrator RAT-IIS, for chlorine, the Laboratory for Organic Elemental Microanalysis, Kyoto University.

Chloro(2,2′:6′,2′′-terpyridine)platinum(II) chloride, ([Pt(trpy)Cl]·Cl), 2a·Cl. Counterion metathesis was accomplished by the addition of a large excess of tetrabutylammonium chloride (TBACl) (ca. 120 mg) to a suspension of chloro(2,2′:6′,2′′-terpyridine)platinum(II) trifluoromethanesulfonate **2a**·OTf[S3] (120 mg, 0.196 mmol) in CH_3CN (10 mL). The suspension was stirred for 30 min at r.t. The resulting orange precipitate was filtered and dried in vacuo to give **2a**·Cl (87 mg, 0.174 mmol) in 89% yield. Crystallization of **2a**·Cl from an CH_3CN solution gave a hydrated solid. M.p.: >290 °C. ^{1}H NMR (600 MHz, DMSO-d_6, r.t.): δ (ppm) 8.97 (d, J = 4.8 Hz, 2H, pyridine-6′-H), 8.60 (m, 5H, pyridine-3,4,2′-H), 8.52 (td, J = 6.0 and 1.8 Hz, 2H, pyridine-3′-H), 7.95 (td, J = 6.0 and 1.2 Hz, 2H, pyridine-5′-H). MALDI-TOF-MS: *m/z* (% intensity): 461.9 (69), 462.9 (84), 463.9 (100), 464.9 (32), 465.9 (36), 466.9 (8), 467.9 (10). Calcd for $C_{15}H_{11}N_3ClPt$ ([M – Cl]$^+$): 464.03. Elemental analysis: calcd (%) for $C_{15}H_{11}N_3Cl_2Pt\cdot 2H_2O$: C 33.66, H 2.82, Cl 13.25, N 7.85; found C 33.65, H 2.83, Cl 13.22, N 7.93.

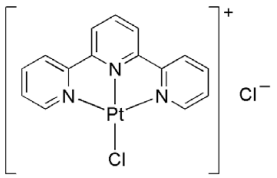

4′-Hexadecyloxy-2,2′:6′,2′′-terpyrdine, trpy-C_{16}. To a solution of 4′-hydroxy-2,2′:6′,2′′-terpyridine (200 mg, 0.802 mmol) and 1-bromohexandecane (245 mg, 0.802 mmol) in DMF (10 mL) was added K_2CO_3 (221 mg, 1.60 mmol). The resulting mixture was stirred for 14 h at 80 °C. CH_2Cl_2 (100 mL) was added to the solution and the resulting precipitate was filtered off. Evaporation of the filtrate under reduced pressure resulted in the precipitation of a colorless crystalline solid. The precipitate was dried in vacuo to give trpy-C_{16} (359 mg, 0.758 mmol) in 94% yield. M.p.: 97–98 °C. ^{1}H NMR (600 MHz, $CDCl_3$, r.t.): δ (ppm) 8.70–8.68 (m, 2H, pyridine-6′-H), 8.62 (d, J = 7.8 Hz, 2H, pyridine-3′-H), 8.01 (s, 2H, pyridine-3-H), 7.85 (td, J = 7.2 and 1.2 Hz, pyridine-4′-H), 7.32 (ddd, J = 7.2, 4.2, and 0.6 Hz, 2H, pyridine-5′-H), 4.22 (t, J = 6.6 Hz, 2H, OCH_2), 1.85 (quin, J = 7.2 Hz, 2H, $OCH_2\underline{CH_2}$), 1.50 (quin, J = 7.2 Hz, 2H, $OC_2H_4\underline{(CH_2)}$), 1.37 (quin, J = 7.2 Hz, $OC_3H_6(\underline{CH_2})$), 1.33–1.26 (m, 22H, $OC_4H_8\underline{(CH_2)_{11}}$), 0.88 (t, J = 7.2 Hz, 3H, $OC_{15}H_{30}\underline{CH_3}$). MALDI-TOF-MS: *m/z* (% intensity): 474.3 (100), 475.3 (31). Calcd for $C_{31}H_{44}N_3O$ ([M + H]$^+$): 474.34. Elemental analysis: calcd (%) for $C_{31}H_{43}N_3O$: C 78.60, H 9.15, N 8.87; found C 78.35, H 9.25, N 8.82.

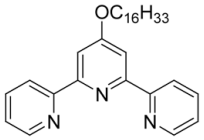

Chloro(4′-hexadecyloxy-2,2′:6′,2′′-terpyridine)platinum(II) trifluoromethanesulfonate, ([Pt(trpy-C_{16})Cl]·OTf), 2b·OTf. To a suspension of $Pt(PhCN)_2Cl_2$ (200 mg, 0.426 mmol) in CH_3CN (15 mL) was added AgOTf (110 mg, 0.426 mmol) in CH_3CN (5 mL). After a 1.5 h reflux and a filtration step, came the addition of 1 equiv of trpy-C_{16} (201 mg, 0.426 mmol) and another 24 h reflux. A second filtration removed any additional AgCl precipitate prior to the removal of the solvent. Evaporation of the solution under reduced pressure resulted in the precipitation of a red solid of **2b**·OTf. The red precipitation was washed with CH_3CN and dried under reduced pressure to give **2b**·OTf (339 mg, 0.397 mmol) in 94% yield. M.p.: 239 °C. ^{1}H NMR (600 MHz, $CDCl_3$, r.t.): δ (ppm) 8.97 (dd, J = 5.4 and 1.2 Hz, 2H, pyridine-6′-H), 8.49 (d, J = 7.2 Hz, 2H, pyridine-3′-H), 8.20 (ddd, J = 7.8, 7.2, and 1.2 Hz, 2H, pyridine-4′-H), 7.94 (s, 2H, pyridine-3-H), 7.66 (dd, J = 7.8 and 5.4 Hz, 2H, pyridine-5′-H), 4.42 (t, J = 6.6 Hz, 2H, OCH_2), 1.99–1.85 (m, 2H, $OCH_2\underline{CH_2}$), 1.57–1.47 (m, 2H, $OC_2H_4\underline{(CH_2)}$), 1.36–1.34 (m, 2H, $OC_3H_6(\underline{CH_2})$), 1.24 (m, 22H, $OC_4H_8\underline{(CH_2)_{11}}$), 0.85 (t, J = 7.2 Hz, 3H, $OC_{15}H_{30}\underline{CH_3}$). ^{19}F NMR (564 MHz, $CDCl_3$, r.t.): δ (ppm) −49.4 (CF_3). MALDI-TOF-MS: *m/z* (% intensity): 701.9 (71), 702.9 (92), 703.9 (100), 704.9 (52), 705.9 (40), 706.9 (11), 707.9 (9). Calcd for $C_{31}H_{43}N_3OClPt$ ([M – OTf]$^+$): 704.27.

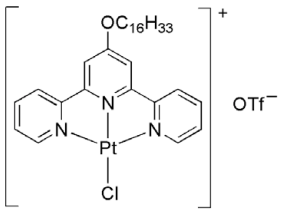

Chloro(4′-hexadecyloxy-2,2′:6′,2′′-terpyridine)platinum(II) chloride ([Pt(trpy-C_{16})Cl]·Cl), 2b·Cl. Counterion metathesis was accomplished by the addition of a large excess of TBACl (ca. 240 mg) to a suspension of **2b**·OTf (640 mg, 0.750 mmol) in CH_3CN (15 mL). The suspension was stirred for 30 min at r.t. The resulting orange crystals were filtered and dried in vacuo to give **2b**·Cl (501 mg, 0.667 mmol) in 91% yield. M.p.: >290 °C. ^{1}H NMR (600 MHz, DMSO-d_6, r.t.): δ (ppm) 8.90 (d, J = 5.4 Hz, 2H, pyridine-6′-H), 8.67 (d, J = 8.4 Hz, 2H, pyridine-3′-H), 8.50 (td, J = 6.6 and 1.2 Hz, 2H, pyridine-4′-H), 8.31 (s, 2H, pyridine-3-H), 7.92 (td, J = 5.4 and 1.2 Hz, 2H, pyridine-5′-H), 4.37 (t, J = 6.6 Hz, 2H, OCH_2), 1.86–1.83 (m, 2H, $OCH_2\underline{CH_2}$), 1.49–1.45 (m, 2H, $OC_2H_4\underline{(CH_2)}$), 1.37–1.36 (m, 2H, $OC_3H_6(\underline{CH_2})$), 1.21 (m, 22H, $OC_4H_8\underline{(CH_2)_{11}}$), 0.83 (t, J = 6.6 Hz, 3H, $OC_{15}H_{30}\underline{CH_3}$). MALDI-TOF-MS: *m/z* (% intensity): 701.9 (77), 702.9 (95), 703.9 (100), 704.9 (48), 705.9 (35), 706.9 (10), 707.9 (8). Calcd for $C_{31}H_{43}N_3OClPt$ ([M – Cl]$^+$): 704.27. Elemental analysis: calcd (%) for $C_{31}H_{43}N_3OCl_2Pt$: C 50.34, H 5.86, Cl 9.59, N 5.68; found C 50.28, H 5.61, Cl 9.32, N 5.78.

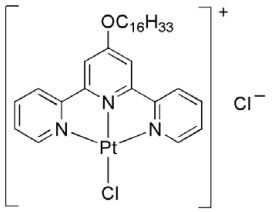

Formation of ion pair 1a·Cl$^-$-2a$^+$. A suspension of **2a**·Cl (7.98 mg, 16.0 μmol) and a slight excess of **1a** (6.70 mg, 16.7 μmol) in CH_3CN (2 mL) was subjected to stirring for 40 min at r.t. The resulting orange precipitate was filtered off, washed with CH_3CN, and dried in vacuo to give **1a**·Cl$^-$-**2a**$^+$ (11.73 mg, 13.0 μmol) in 81% yield. The formation of 1:1 ion pair (**1a**·Cl$^-$-**2a**$^+$) was confirmed by ^{1}H NMR spectroscopy (Supporting Figure 1a) and elemental analysis. Elemental analysis: calcd (%) for $C_{38}H_{28}BN_5O_2F_2Cl_2Pt$: C 50.63, H 3.13, N 7.77; found C 50.41, H 3.38, N 7.94 (for the species containing B, the exact value of this element along with Cl and F cannot be estimated).

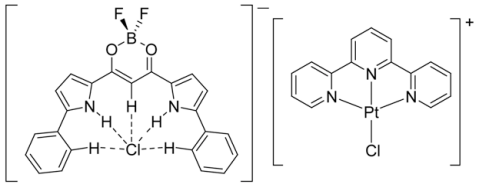

Preparation of 1b·Cl$^-$-2a$^+$. A suspension of **2a**·Cl (1.34 mg, 2.68 μmol) and a slight excess of **1b** (5.00 mg, 2.71 μmol) in 1,4-dioxane (1 mL) was subjected to stirring for 50 min at r.t. The resulting red precipitate was filtered off, washed with 1,4-dioxane, and dried in vacuo to give **1b**·Cl$^-$-**2a**$^+$ (5.12 mg, 2.18 μmol) in 81% yield. The formation of 1:1 ion pair (**1b**·Cl$^-$-**2a**$^+$) was confirmed by ^{1}H NMR spectroscopy (Supporting Figure 1b) and elemental analysis. Elemental analysis: calcd (%) for $C_{134}H_{220}BN_5O_8F_2Cl_2Pt$: C 68.66, H 9.46, N 2.99; found C 68.39, H 9.66, N 2.75 (for the species containing B, the exact value of this element along with Cl and F cannot be estimated).

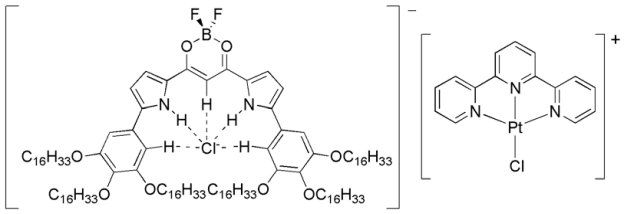

Formation of ion pair 1b·Cl$^-$-2b$^+$. A suspension of **2b**·Cl (4.7 mg, 6.3 μmol) and a slight excess of **1b** (11.8 mg, 6.4 μmol) in 1,4-dioxane (2 mL) was subjected to stirring for 20 min at r.t. The resulting red precipitate was filtered off, washed with 1,4-dioxane, and dried in vacuo to give **1b**·Cl$^-$-**2b**$^+$ (13.6 mg, 5.26 μmol) in 83% yield. The formation of 1:1 ion pair (**1b**·Cl$^-$-**2b**$^+$) was confirmed by ^{1}H NMR spectroscopy (Supporting Figure 1c) and elemental analysis. Elemental analysis: calcd (%) for $C_{150}H_{252}BN_5O_9F_2Cl_2Pt$: C 69.71, H 9.83, N 2.71; found C 69.69, H 9.83, N 2.70 (for the species containing B, the exact value of this element along with Cl and F cannot be estimated).

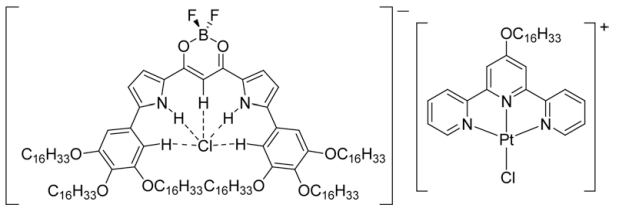

Formation of ion pair 1b′·Cl$^-$-2a$^+$. A suspension of **2a**·Cl (6.48 mg, 13.0 μmol) and a slight excess of **1b′** (8.37 mg, 14.4 μmol) in CH_3CN (1 mL) was subjected to stirring for 40 min at r.t. The resulting red precipitate was filtered off, washed with CH_3CN, and dried in vacuo to give **1b′**·Cl$^-$-**2a**$^+$ (11.40 mg, 10.6 μmol) in 81% yield. The formation of 1:1 ion pair (**1b′**·Cl$^-$-**2a**$^+$) was confirmed by ^{1}H NMR spectroscopy (Supporting Figure 1d).

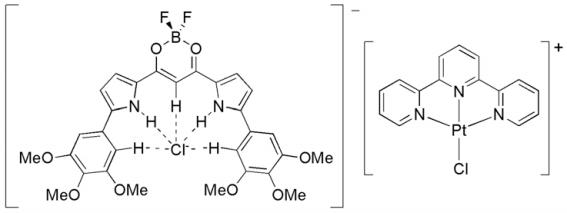

[S1] H. Maeda and Y. Kusunose, *Chem. Eur. J.*, 2005,

11, 5661–5666.

[S2] H. Maeda, Y. Haketa and T. Nakanishi, *J. Am. Chem. Soc.*, 2007, **129**, 13661–13674.

[S3] R. Büchner, J. S. Field and R. J. Haines, *Inorg. Chem.*, 1997, **36**, 3952–3956.

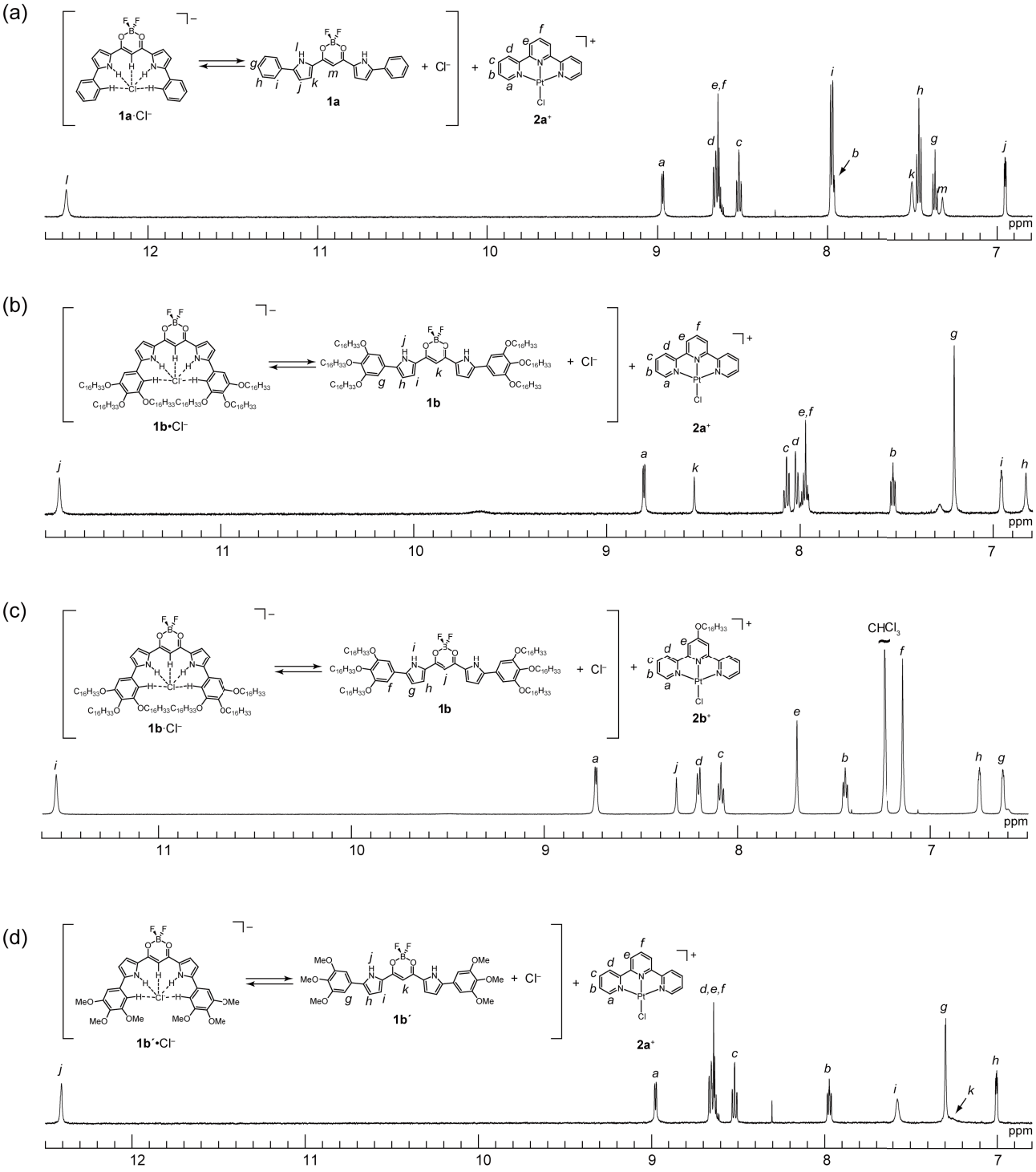

Supporting Figure 1 Partial views of ^{1}H NMR spectra of (a) **1a**·Cl$^-$-**2a**$^+$ in DMSO-d_6, (b) **1b**·Cl$^-$-**2a**$^+$ in CD_2Cl_2, (c) **1b**·Cl$^-$-**2b**$^+$ in $CDCl_3$, and (d) **1b´**·Cl$^-$-**2a**$^+$ in DMSO-d_6. The anion receptors are observed as their Cl$^-$ complexes, even though the labels are located in the structures of anion-free forms. ^{1}H NMR spectra of (a), (c), and (d) suggest the presence of the receptors (**1a**, **1b**, and **1b´**) and the platinum salts (**2a**·Cl and **2b**·Cl) in the 1:1 ratio. As observed in (b), a small amount of **2a**·Cl was precipitated without the formation of the ion pair due to the less solubility of the platinum salt in CD_2Cl_2. However, elemental analysis of the solid-state **1b**·Cl$^-$-**2a**$^+$, which was obtained by the precipitation of the ion pair from a 1,4-dioxane solution, demonstrated the presence of **1b** and **2a**·Cl in the 1:1 ratio.

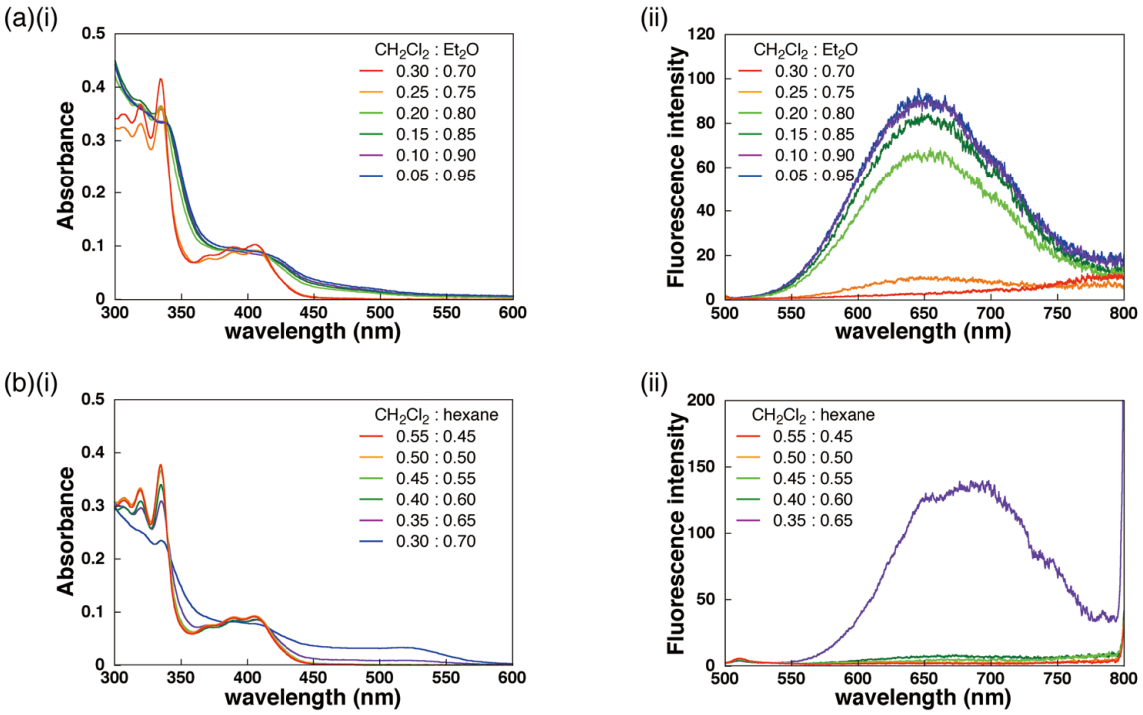

Supporting Figure 2 (i) UV/vis absorption and (ii) fluorescence spectra of **2b**·Cl (2.77×10^{-5} M) in the mixed solvents of (a) CH_2Cl_2 (λ_{ex} = 420 nm) and Et_2O (λ_{ex} = 406 nm) and (b) CH_2Cl_2 and hexane. Solution-state UV/vis absorption spectra in the mixed solvents suggested the aggregation behavior of **2b**$^+$ in less polar solvents, wherein the new absorption bands at low-energy region and emission bands were observed due to the existence of $Pt^{II}\cdots Pt^{II}$ interaction in the aggregated **2b**$^+$.

2. X-ray crystallographic data

Single-crystal X-ray analysis. Crystallographic data is summarized in Supporting Table 1. A single crystal of **1c**·Cl^--**2a**$^+$ was obtained by slow evaporation of an CH_3CN solution of **1c**, diphenylboron complex of 1,3-di(5-phenylpyrrol-2-yl)-1,3-propanedione,[S4] and **2a**·Cl in an equivalent ratio. The data crystal of **1c**·Cl^--**2a**$^+$ was an orange platelet crystal of approximate dimensions 0.10 mm × 0.10 mm × 0.05 mm. Data was collected at 93 K on a Rigaku RAXIS-RAPID II diffractometer with graphite monochromated Cu-Kα radiation (λ = 1.54187 Å). The structures were solved by direct method using *SIR-2004*[S5] and refined by the successive differential Fourier syntheses and full-matrix least squares procedure using *SHELXL-97*.[S6] The non-hydrogen atoms were refined anisotropically. The calculation was performed using the Crystal Structure crystallographic software package of Molecular Structure Corporation.[S7] CIF file (CCDC-988279) can be obtained free of charge from the Cambridge Crystallographic Data Centre via www.ccdc.cam.ac.uk/data_request/cif.

Supporting Table 1 Crystallographic data for **1c**·Cl^--**2a**$^+$.

	1c·Cl^--**2a**$^+$
formula	$C_{50}H_{38}N_5O_2Cl_2Pt$
fw	1607.4
crystal size, mm	0.10 × 0.10 × 0.05
crystal system	Monoclinic
space group	$P2_1/c$ (no. 14)
a, Å	12.2811(2)
b, Å	12.5617(2)
c, Å	26.9413(5)
α, °	90
β, °	100.943(1)
γ, °	90
V, Å^3	4080.70(8)
ρ_{calcd}, g cm^{-3}	2.62
Z	4
T, K	93
μ (Cu-Kα), mm^{-1}	8.466
no. of reflections	33017
no. of unique reflections	7324
R_{int}	0.097
no. of observed reflns	5652
variables	550
$\lambda_{Cu\text{-}K\alpha}$, Å	1.54187
R_1 ($I > 2\sigma(I)$)	0.056
wR_2 ($I > 2\sigma(I)$)	0.126
GOF	1.017
CCDC	988279

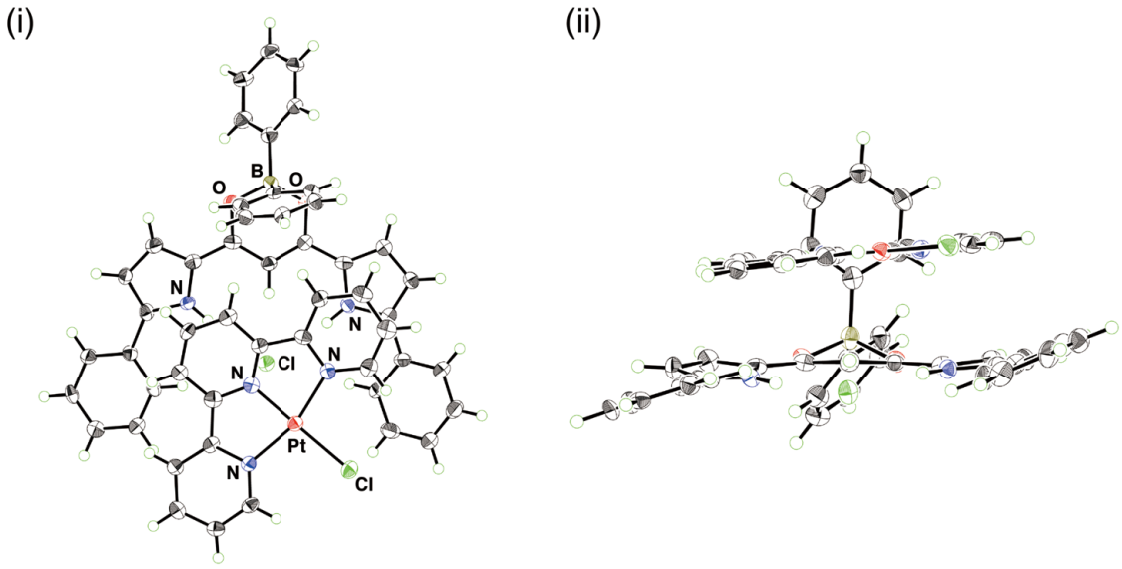

Supporting Figure 3 ORTEP drawings ((i) top and (ii) side view) of single-crystal X-ray structure of **1c**·Cl$^-$-**2a**$^+$. Thermal ellipsoids are scaled to the 50% probability level. Atom color code: gray (carbon), white (hydrogen), pink (boron), blue (nitrogen), red (oxygen), dark green (chlorine), and silver (platinum).

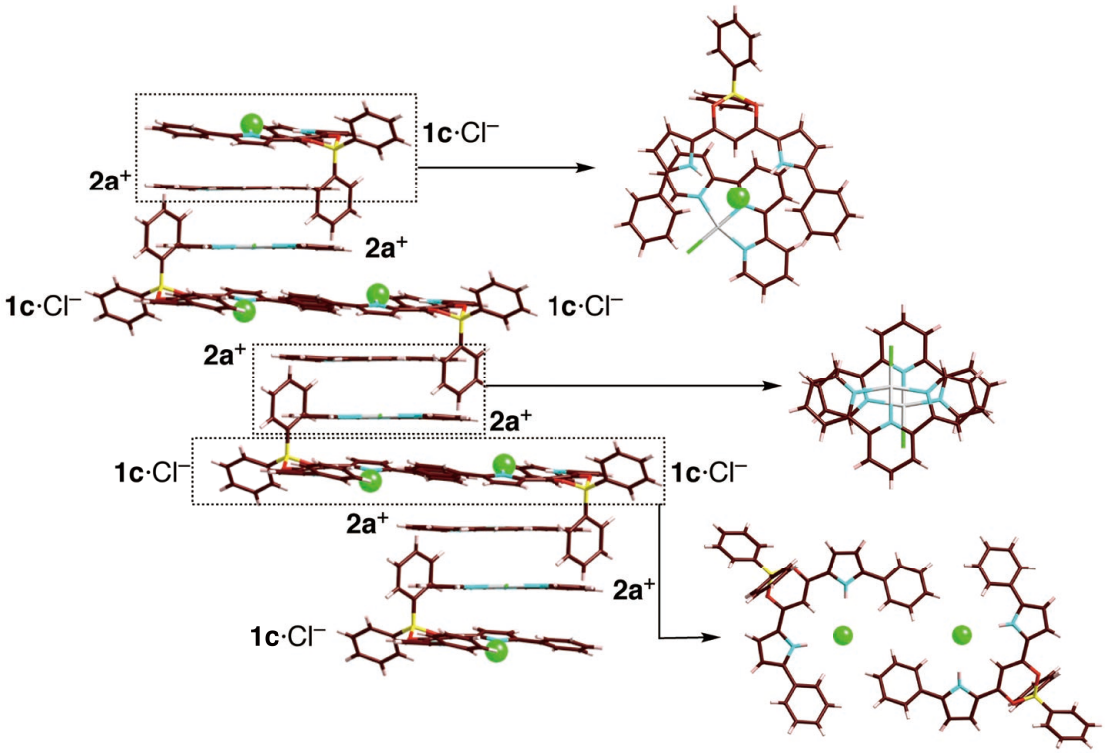

Supporting Figure 4 Solid-state assembled structure of **1c**·Cl$^-$-**2a**$^+$. Atom color code: brown (carbon), pink (hydrogen), yellow (boron), blue (nitrogen), red (oxygen), dark green (chlorine), and silver (platinum). We prepared single crystals of an ion pair consisting of **1c**·Cl$^-$ and **2a**$^+$ for investigating the effect of the substituents on the boron atom of the anion receptor on the formation of charge-based assemblies. Although **2a**$^+$ form the Pt^{II} dimer with Pt$^{II}\cdots$Pt^{II} interaction of 3.476 Å, two **1c**·Cl$^-$ are placed on top and bottom of the Pt^{II} dimer and, as a result, no 1D columnar stacking structure of Pt^{II} complexes is formed. Most likely, this is due to the two bulky phenyl rings on the boron atom which prevent the formation of the 1D columnar stacking structure of **2a**$^+$. The result of the crystal structure of the ion pair, **1c**·Cl$^-$-**2a**$^+$, strongly suggest that anion receptors possessing sterically less hindered substituents on the boron atom are suitable for constructing the packing structures exhibiting more contribution of charge-segregated assemblies.

[S4] H. Maeda, M. Takayama, K. Kobayashi and H. Shinmori, *Org. Biomol. Chem.*, 2010, **8**, 4308–4315.
[S5] M. C. Burla, R. Caliandro, M. Camalli, B. Carrozzini, G. L. Cascararo, L. De Caro, C. Giacovazzo, G. Polidori

and R. Spagna, *J. Appl. Cryst.*, 2005, **38**, 381–388
[S6] G. M. Sheldrick, *Acta Crystallogr.*, 2008, **A64**, 112.
[S7] *CrystalStructure* (Ver. 3.8), Single Crystal Structure Analysis Software, Rigaku/MSC and Rigaku Corporation, 2006.

3. Geometry Optimization and Electrostatic Potential Calculations

Geometry optimizations. The optimized structures of **1a**·Cl^- at B3LYP/6-31+G(d,p) level and **1b**·Cl^- at the AM1 method were previously reported.[S2,8] Geometry optimization of $\mathbf{2a}^+$ was carried out using the 6-31G(d,p) and LanL2DZ mixed basis set coupled with B3LYP.[S9] The 6-31G(d,p) basis set was used for H, C, N, and O atoms, whereas the LanL2DZ basis set was used for Pt. Geometry optimization of $\mathbf{2b}^+$ was carried out using the PM6 method.[S10]

Electrostatic potential calculations. The electrostatic potential of **1a**·Cl^- at B3LYP/6-31+G(d,p) level was previously reported.[S11] Estimation of the electrostatic potential of $\mathbf{2a}^+$ using the optimized structure of $\mathbf{2a}^+$ was carried out using the 6-31G+(d,p) + LanL2DZ mixed basis set coupled with B3LYP. Mapping of electrostatic potentials and graphical outputs were done using the *MOLEKEL* ver. 5.4 Program.[S12]

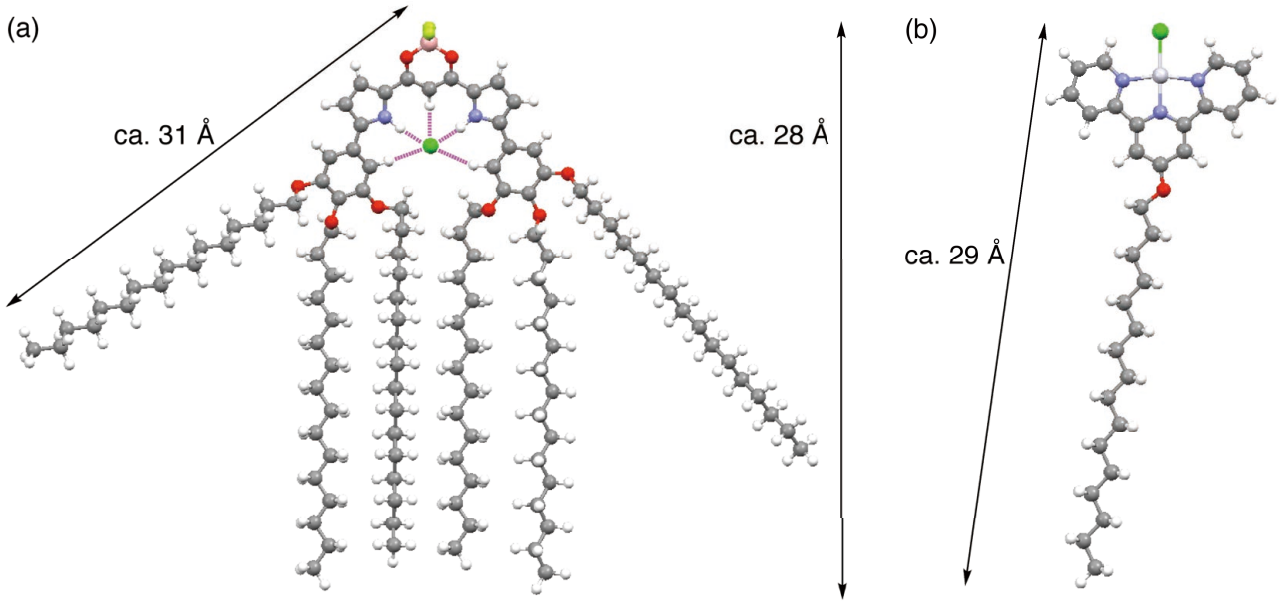

Supporting Figure 5 Optimized structures of (a) **1b**·Cl^- at AM1[S8] and (b) $\mathbf{2b}^+$ at PM6 level. Atom color code: gray (carbon), white (hydrogen), pink (boron), blue (nitrogen), red (oxygen), yellowish-green (fluorine), green (chlorine), and silver (platinum).

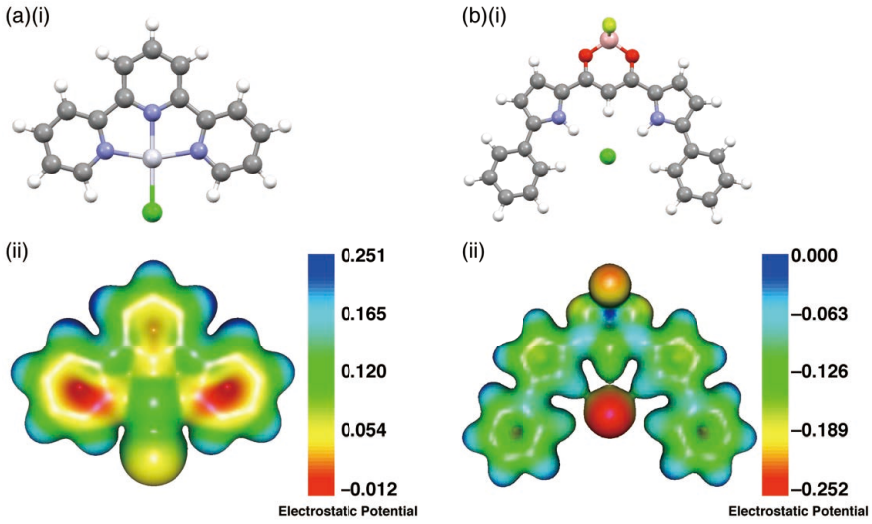

Supporting Figure 6 (i) Optimized structures and (ii) electron density diagrams of (a) $\mathbf{2a}^+$ and (b) **1a**·Cl^-.[S2,11] Electrostatic potentials were mapped onto the electron density isosurface (δ = 0.02) calculated at B3LYP/6-31+G(d,p) + LanL2DZ for $\mathbf{2a}^+$, at B3LYP/6-31+G(d,p) for **1a**·Cl^-. The LanL2DZ basis set was employed to assign the Pt atom. Atom color code: gray (carbon), white (hydrogen), pink (boron), blue (nitrogen), red (oxygen), yellowish green (fluorine), green (chlorine), and silver (platinum).

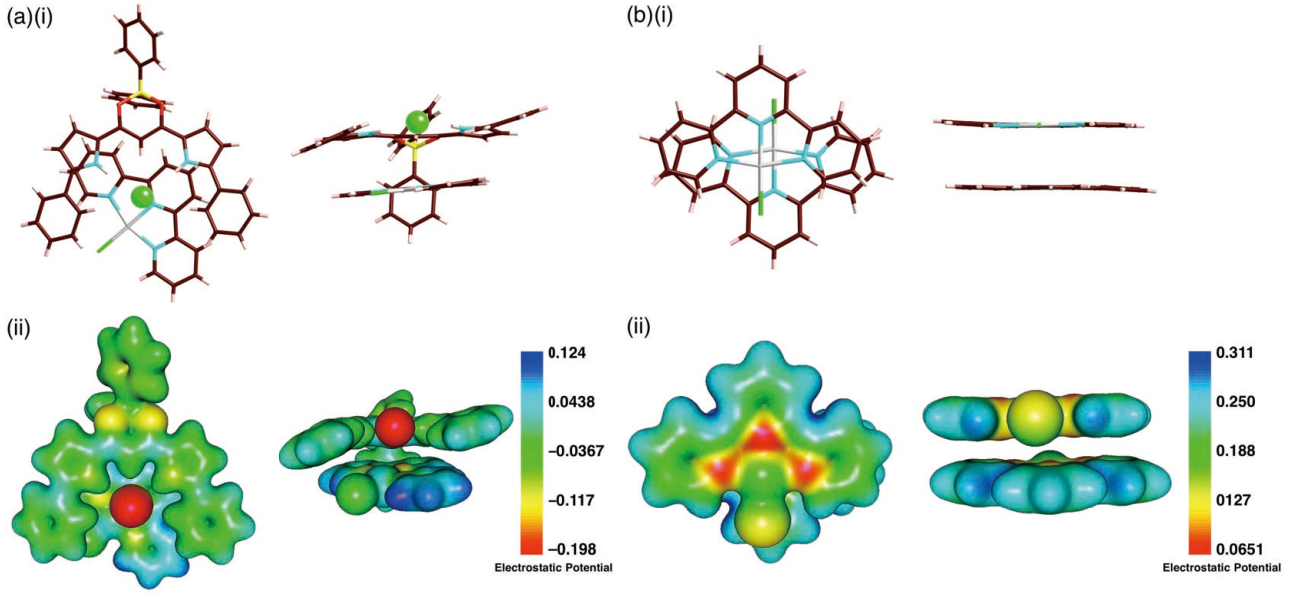

Supporting Figure 7 Electron density diagram of (a) stacking ions pair comprising **1c**·Cl^--**2a**$^+$ and (b) stacking cation dimer (**2a**$^+$)$_2$ found in the crystal of **1c**·Cl^--**2a**$^+$. Electrostatic potentials were mapped onto the electron density isosurface (δ = 0.02) calculated at B3LYP/6-31+G(d,p) + LanL2DZ for the crystal structure. The LanL2DZ basis set was employed to assign the Pt atom. Atom color code: gray (carbon), white (hydrogen), pink (boron), blue (nitrogen), red (oxygen), yellowish green (fluorine), green (chlorine), and silver (platinum). The electrostatic potential maps in (a) and (b) represent the situation of the contributions of charge-by-charge and charge-segregated assemblies, respectively. As for the planar cation **2a**$^+$, the electrostatic potential in (a) showed the partial delocalization to the receptor–anion complex, which is in contrast to that in (b).

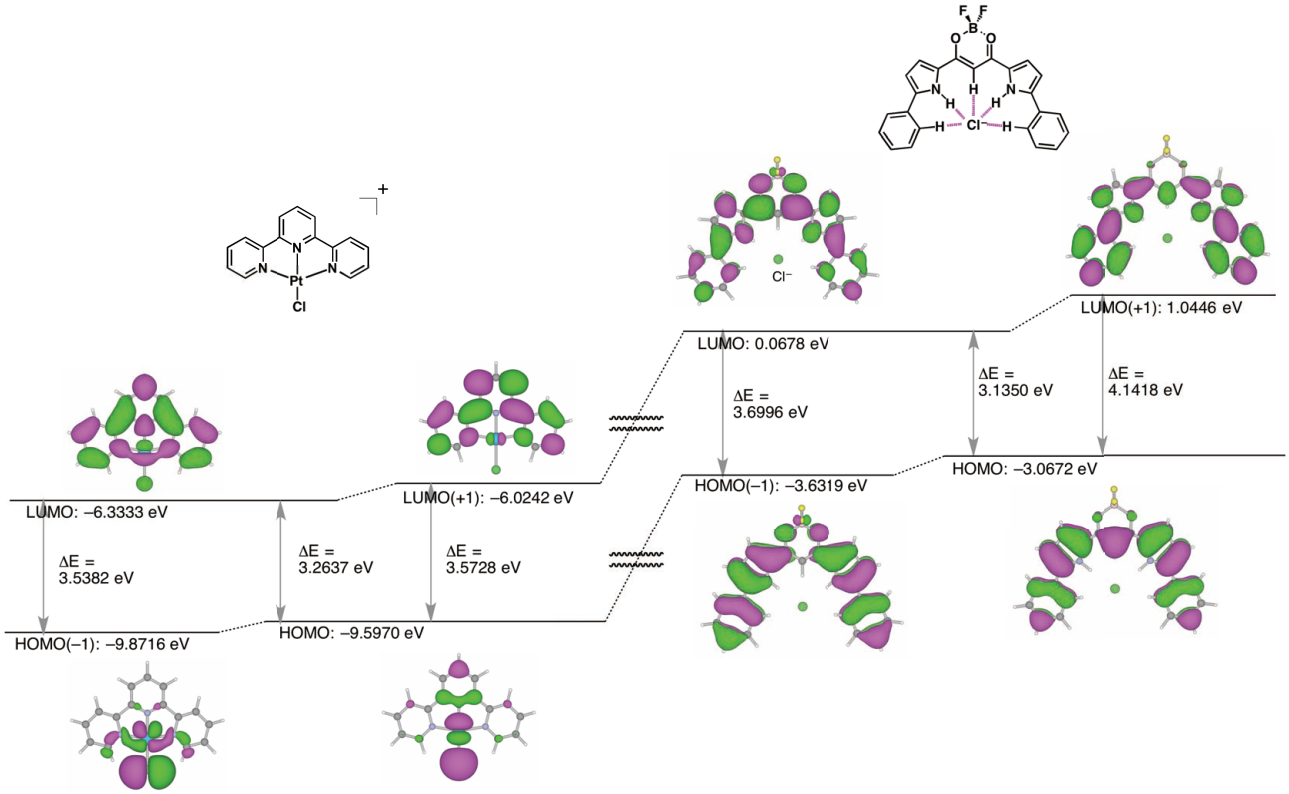

Supporting Figure 8 Energy level diagram of **2a**$^+$ and **1a**·Cl^-[S2,11] at B3LYP/6-31+G(d,p) + LanL2DZ for **2a**$^+$, at B3LYP/6-31+G(d,p) for **1a**·Cl^-. The LanL2DZ basis set was employed to assign the Pt atom. The calculated molecular orbitals may be correlated with the locations of charge carrier generations on the examination of the semi-conductive properties.

Cartesian Coordination of $2a^+$

−1321.7522024 hartree

Cl,-0.0000130575,0.0000092836,-3.047853384
H,0.0000372832,-0.0000430659,5.0649422509
H,2.1522737172,-0.0005566626,3.8364374497
H,-2.1522313554,0.000499883,3.8364570512
H,3.9336509854,-0.0009623366,2.4175983604
H,5.7297899089,-0.0013796151,0.6992514892
H,2.6483340437,-0.0006086856,-2.3310819642
H,5.0921456697,-0.0012121653,-1.7304970374
H,-3.9336282321,0.0009645723,2.417637927
H,-5.7297701216,0.0014259713,0.6993294666
H,-2.6483461787,0.0006751342,-2.3310468529
H,-5.0921459629,0.0012756154,-1.7304515678
N,-2.0241598545,0.0005123014,-0.3710271773
N,0.0000063833,-0.0000147051,1.2666204861
N,2.0241672705,-0.0004587479,-0.3710504111
Pt,-0.0000106255,-0.0000100592,-0.699001262
C,1.2158820473,-0.0003229538,3.291621835
C,2.3475172879,-0.0005842404,0.9648419238
C,-4.3395740877,0.0010824776,-0.9503483236
C,-3.6800325046,0.0009019249,1.3639745278
C,-4.6878582943,0.0011556655,0.3968811589
C,-2.990042645,0.0007544593,-1.3016997332
C,-1.1962894543,0.0002786804,1.8959466408
C,-2.3475009909,0.0005672706,0.9648818345
C,1.1963177848,-0.0003082918,1.8959330342
C,-1.2158368068,0.0002686373,3.2916470941
C,3.6800562898,-0.0008924593,1.3639353078
C,4.687867488,-0.0011148763,0.3968359936
C,2.9900415163,-0.0006762993,-1.3017385818
C,4.339569646,-0.0010280892,-0.950397341
C,0.0000234598,-0.0000358698,3.9802228135

Cartesian Coordination of $2b^+$ (PM6)

120.2437 hartree

N,0.0000,0.0000,0.0000
C,1.3870,0.0000,0.0000
C,-0.7600,1.1480,0.0000
C,-0.1250,2.3880,0.0000
C,2.0580,1.2080,0.0000
C,1.2910,2.4150,0.0000
C,-2.2140,0.8290,0.0000
H,-0.7060,3.3090,0.0000
C,1.9250,-1.3880,-0.0010
H,3.1500,1.2780,0.0010
O,2.0550,3.5150,0.0000
N,-2.5140,-0.5430,-0.0010
C,-3.2320,1.7770,0.0000
C,-4.5740,1.3490,-0.0010
C,-3.8090,-0.9490,-0.0010
C,-4.8610,-0.0110,-0.0010
H,-2.9990,2.8460,0.0000
H,-5.3820,2.0910,0.0000
H,-4.0060,-2.0410,-0.0010
H,-5.8980,-0.3710,-0.0010
N,0.9500,-2.3980,-0.0010
C,3.2790,-1.7080,-0.0010
C,3.6680,-3.0620,-0.0010
C,1.3310,-3.7000,-0.0010
C,2.6960,-4.0550,-0.0010
H,4.0390,-0.9200,-0.0002
H,4.7330,-3.3220,-0.0010
H,0.5320,-4.4710,-0.0010
H,2.9710,-5.1170,-0.0020
C,1.4250,4.8580,0.0000
Pt,-0.9020,-1.6920,-0.0010
Cl,-1.9913,-3.7354,-0.0022
H,0.8150,4.9470,-0.9140
H,0.8100,4.9450,0.9110
C,2.6410,5.7730,0.0050
H,3.2710,5.5700,0.8970
H,3.2920,5.5500,-0.8670
C,2.2070,7.2450,-0.0170
H,1.5910,7.4500,-0.9140
H,1.5640,7.4690,0.8570
C,3.4270,8.1760,-0.0090
H,4.0510,7.9810,0.8860
H,4.0760,7.9620,-0.8810
C,3.0020,9.6510,-0.0310
H,2.3820,9.8550,-0.9250
H,2.3570,9.8740,0.8420
C,4.2210,10.5830,-0.0240
H,4.8450,10.3850,0.8700
H,4.8690,10.3670,-0.8960
C,3.7980,12.0570,-0.0440
H,3.1760,12.2610,-0.9380
H,3.1540,12.2790,0.8280
C,5.0170,12.9890,-0.0380
H,5.6410,12.7900,0.8550
H,5.6630,12.7730,-0.9110
C,4.5950,14.4650,-0.0580
H,3.9720,14.6670,-0.9500
H,3.9510,14.6850,0.8150
C,5.8140,15.3970,-0.0530
H,6.4380,15.1970,0.8400
H,6.4590,15.1790,-0.9260
C,5.3920,16.8720,-0.0720
H,4.7680,17.0740,-0.9640
H,4.7480,17.0920,0.8010
C,6.6110,17.8040,-0.0670
H,7.2360,17.6040,0.8250
H,7.2560,17.5860,-0.9410
C,6.1890,19.2790,-0.0860
H,5.5650,19.4810,-0.9780
H,5.5460,19.4990,0.7870
C,7.4090,20.2110,-0.0820
H,8.0340,20.0110,0.8090
H,8.0540,19.9950,-0.9550
C,6.9879,21.6870,-0.1010
H,6.3639,21.8900,-0.9930
H,6.3449,21.9070,0.7740
C,8.1979,22.6190,-0.0970
H,8.8189,22.4720,0.7949
H,8.8379,22.4550,-0.9710
H,7.8879,23.6700,-0.1101

[S8] Y. Haketa, S. Sasaki, N. Ohta, H. Masunaga, H. Ogawa, F. Araoka, H. Takezoe and H. Maeda, *Angew. Chem. Int. Ed.*, 2010, **49**, 10079–10083.

[S9 (Complete ref. 10a)] M. J. Frisch, G. W. Trucks, H. B. Schlegel, G. E. Scuseria, M. A. Robb, J. R. Cheeseman, J. A. Montgomery, Jr., T. Vreven, K. N. Kudin, J. C. Burant, J. M. Millam, S. S. Iyengar, J. Tomasi, V. Barone, B. Mennucci, M. Cossi, G. Scalmani, N. Rega, G. A. Petersson, H. Nakatsuji, M. Hada, M. Ehara, K. Toyota, R. Fukuda, J. Hasegawa, M. Ishida, T. Nakajima, Y. Honda, O. Kitao, H. Nakai, M. Klene, X. Li, J. E. Knox, H. P. Hratchian, J. B. Cross, C. Adamo, J. Jaramillo, R. Gomperts, R. E. Stratmann, O. Yazyev, A. J. Austin, R. Cammi, C. Pomelli, J. W. Ochterski, P. Y. Ayala, K. Morokuma, G. A. Voth, P. Salvador, J. J. Dannenberg, V. G. Zakrzewski, S. Dapprich, A. D. Daniels, M. C. Strain, O. Farkas, D. K. Malick, A. D. Rabuck, K. Raghavachari, J. B. Foresman, J. V. Ortiz, Q. Cui, A. G. Baboul, S. Clifford, J. Cioslowski, B. B. Stefanov, G. Liu, A. Liashenko, P. Piskorz, I. Komaromi, R. L. Martin, D. J. Fox, T. Keith, M. A. Al-Laham, C. Y. Peng, A. Nanayakkara, M. Challacombe, P. M. W. Gill, B. Johnson, W. Chen, M. W. Wong, C. Gonzalez and J. A. Pople, Gaussian, Inc., Wallingford CT, 2004.

[S10] *MOPAC2012*, J. J. P. Stewart, Stewart Computational Chemistry, Colorado Springs, CO, 2012.

[S11] Y. Haketa, Y. Honsho, S. Seki and H. Maeda, *Chem*. *Eur*. *J*., 2012, **18**, 7016–7020.

[S12] *MOLEKEL 5.4*, U. Varetto, Swiss National Supercomputing Centre, Manno, Switzerland.

4. Formation of charge-based assemblies

Differential Scanning Calorimetry (DSC). The phase transitions were measured on a differential scanning calorimetry (Perkin-Elmer Diamond DSC).

Polarized Optical Microscopy (POM). The textures were observed by using a polarization microscope (Nikon ECLIPSE E600 POL), equipped with a heating plate (Mettler FP-82 HT hot stage) controlled by a thermoregulator (Mettler FP-90 Central Processor).

Synchrotron X-ray Diffraction (XRD) Analysis. High-resolution XRD analyses were carried out using a synchrotron radiation X-ray beam with a wavelength of 1.00 Å on BL40B2 at Spring-8 (Hyogo, Japan). A large Debye-Scherrer camera with a camera length of 540.18 nm was used with an imaging plate as a detector. The sample was sealed in a quartz capillary where the diffraction pattern was obtained with a 0.01° step in 2θ under the exposure time of 30 s.

UV/vis absorption measurement. UV-visible spectra were recorded on a Hitachi U-3500 spectrometer for ordinary solution and solid-state samples.

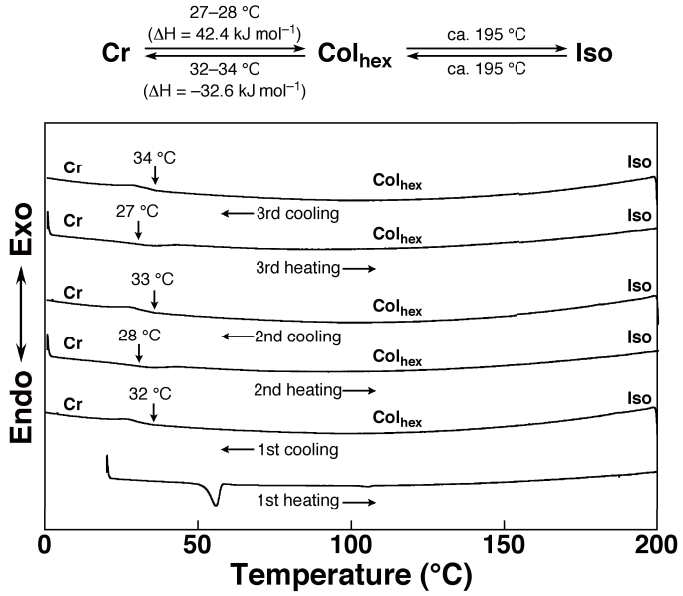

Supporting Figure 9 DSC thermograms of **1b**·Cl^--**2b**$^+$ on the 1st heating/cooling, 2nd heating/cooling, and 3rd heating/cooling. Onset temperatures (°C) of phase transitions (Cr ↔ Col_{hex}) are labeled. Onset temperatures (°C) of phase transitions (Col_{hex} ↔ Iso) are too weak to be detected, whereas POM measurements (Supporting Figure 10) suggest that the phase transitions (Col_{hex} ↔ Iso) occur at ca. 195 °C. Phase nomenclature: Cr = crystal, Col_{hex} = hexagonal columnar mesophase, and Iso = isotropic liquid.

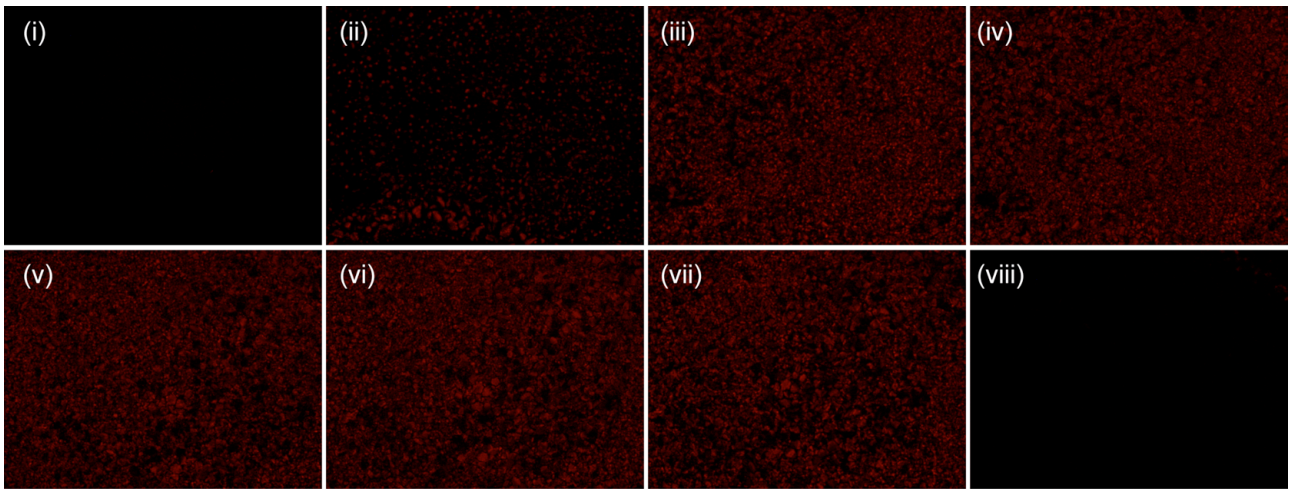

Supporting Figure 10 POM textures of **1b**·Cl^{-}-**2b**$^{+}$ at (i) 200 °C (1st heating, Iso), (ii) 185 °C (1st cooling, Col$_{hex}$), (iii) 160 °C (1st cooling, Col$_{hex}$), (iv) 120 °C (1st cooling, Col$_{hex}$), (v) 35 °C (1st cooling, Col$_{hex}$), (vi) 120 °C (2nd heating, Col$_{hex}$), (vii) 160 °C (2nd heating, Col$_{hex}$), and (viii) 200 °C (2nd heating, Iso).

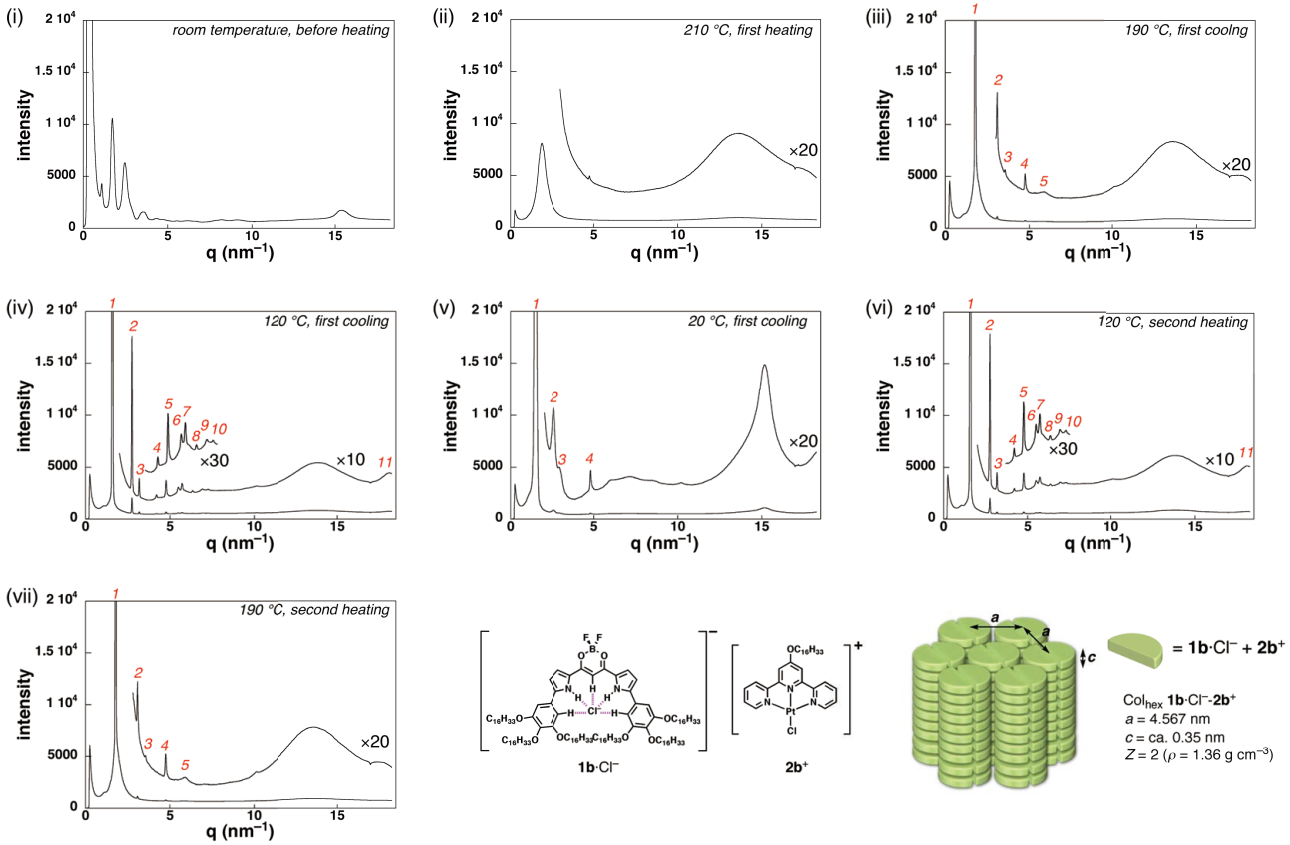

Supporting Figure 11 XRD patterns of **1b**·Cl^{-}-**2b**$^{+}$ at (i) 20 °C, (ii) 210 °C, (iii) 190 °C, (iv) 120 °C, (v) 20 °C, (vi) 120 °C, and (vii) 190 °C upon (i–iii) 1st heating, (iv, v) 1st cooling, and (vi,vii) 2nd heating. The assumed ρ value was based on the single-crystal X-ray structures of some reported Pt^{II} complexes possessing large organic parts, such as a compound composed of uracil and organoplatinium moiety. The reported ρ value of the crystal of the Pt^{II} complex is 1.57 g cm^{-3}, and the ratio of C, H, N, and O to Pt of the Pt^{II} complex ($C_{38.5}H_{47}N_4O_3ClPt$) is lower than that of **1b**·Cl^{-}-**2b**$^{+}$ ($C_{150}H_{252}N_5O_9BF_2Cl_2Pt$). Thus, the ρ value of **1b**·Cl^{-}-**2b**$^{+}$ in the Col$_{hex}$ mesophase must be lower than but fairly close to 1.57 g cm^{-3}. See ref 8g in the manuscript.[S13]

Supporting Table 2 Summary of XRD data of **1b**·Cl^--**2b**$^+$. The peaks which can be indexed are represented.

	peak no.	q (nm^{-1})	*d*-spacing (nm)	ratio	*hkl*
(iii) 190 °C upon 1st cooling (Col_{hex})	1	1.774	3.542	1	100
	2	3.086	2.036	0.575	110
	3	3.553	1.768	0.499	200
	4	4.751	1.322	0.373	210
	5	5.892	1.066	0.303	300, 220
(iv) 120 °C upon 1st cooling (Col_{hex})	1	1.591	3.949	1	100
	2	2.755	2.281	0.578	110
	3	3.177	1.978	0.501	200
	4	4.203	1.495	0.379	210
	5	4.762	1.319	0.334	300
	6	5.504	1.142	0.289	220
	7	5.721	1.098	0.278	310
	8	6.348	0.990	0.251	400
	9	6.930	0.907	0.230	320
	10	7.272	0.864	0.219	410
	11	18.108	0.347	–	001
(v) 20 °C upon 1st cooling (Col_{hex} in Cr)	1	1.477	4.253	1	100
	2	2.572	2.443	0.574	110
	3	2.914	2.156	0.507	200
	4	4.808	1.307	0.307	300
(vi) 120 °C upon 2nd heating (Col_{hex})	1	1.591	3.949	1	100
	2	2.755	2.281	0.578	110
	3	3.177	1.978	0.501	200
	4	4.203	1.495	0.379	210
	5	4.774	1.316	0.333	300
	6	5.504	1.142	0.289	220
	7	5.732	1.096	0.278	310
	8	6.359	0.988	0.250	400
	9	6.918	0.908	0.230	320
	10	7.283	0.863	0.218	410
	11	18.142	0.346	–	001
(vii) 190 °C upon 2nd heating (Col_{hex})	1	1.785	3.519	1	100
	2	3.086	2.036	0.579	110
	3	3.553	1.768	0.502	200
	4	4.751	1.322	0.376	210
	5	5.892	1.066	0.303	300, 220

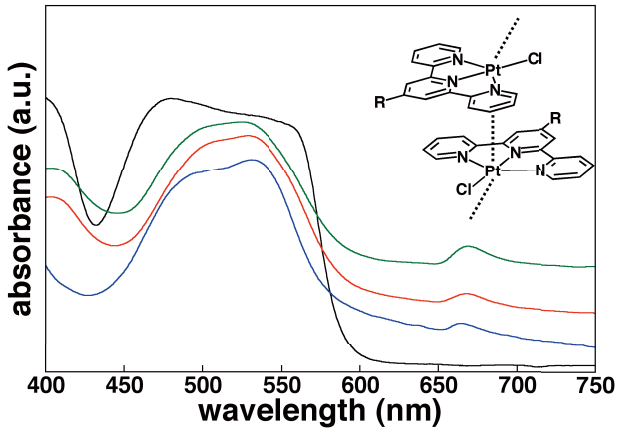

Supporting Figure 12 Solid-state UV/vis absorption spectra of **1a**·Cl^--**2a**$^+$ (blue: r.t.), **1b**·Cl^--**2b**$^+$ (red: r.t.; green: 100 °C), and **1b**·Cl^--TBA^+ (black: r.t.) and a schematic representation of stacking Pt^{II} complexes with $Pt^{II}\cdots Pt^{II}$ interaction (dotted line) (inset). Before the solid-state UV/vis measurement, ion pair **1b**·Cl^--**2b**$^+$ was annealed at 200 °C for 5 min. Square-planar Pt^{II} complexes often form dimer-based 1D stacking columnar with short $Pt^{II}\cdots Pt^{II}$ contacts.[S13–16] This metallophilicity is attributable in part to bonding interactions arising from the overlap of the $5d_{z^2}$ and $6p_z$ orbitals of adjacent Pt^{II} centers.[S14a,16c] The interaction between the fully occupied $5d_{z^2}$ orbitals gives bonding (dσ) and antibonding (dσ*) molecular orbitals; similarly, interaction between the unoccupied $6p_z$ orbitals gives pσ and pσ* molecular orbitals. Since both dσ and dσ* orbitals are fully occupied, no formal bonding occurs. However, configuration interaction with the pσ and pσ* orbitals stabilizes the dσ and dσ* levels, resulting in net favorable interactions. The aggregated Pt^{II} complexes exhibit characteristic absorption bands at low energy region due to the dσ*(Pt_2) → π*(trpy) metal-metal-to-ligand charge transfer (MMLCT).[S14,15a,c]

[S13] T. Moriuchi, Y. Sakamoto, S. Noguchi, T. Fujiwara, S. Akine, T. Nabeshima and T. Hirao, *Dalton Trans*., 2012, **41**, 8524–8531.

[S14] (a) K. Krogman, *Angew. Chem. Int. Ed. Engl*., 1969, **8**, 35–42; (b) T. W. Thomas and A. E. Underhill, *Chem. Soc. Rev*., 1972, **1**, 99–120.

[S15] (a) I. Eryazici, C. N. Moorefield and G. R. Newkome, *Chem. Rev*., 2008, **108**, 1834–1895; (b) S. D. Cummings, *Coord. Chem. Rev*., 2009, **253**, 449–478; (c) V. W.-W. Yam and K. M.-C. Wong, *Chem. Commun*., 2011, **47**, 11579–11592.

[S16] (a) J. A. Bailey, M. G. Hill, R. E. Marsh, V. M. Misokowski, W. P. Schaefer and H. B. Gray, *Inorg. Chem*., 1995, **34**, 4591–4599; (b) W. B. Connick, L. M. Henling, R. E. Marsh and H. B. Gray, *Inorg. Chem*., 1996, **35**, 6261–6265; (c) W. B. Connick, R. E. Marsh, W. P. Scaefer and H. B. Gray, *Inorg. Chem*., 1997, **36**, 913–922; (d) V. W.-W. Yam, K. M.-C. Wong and N. Zhu, *J. Am. Chem. Soc*., 2002, **124**, 6506–6507; (e) T. J. Wadas, Q.-M. Wang, T. Kim, C. Flaschenreim, T. N. Blanton and R. Esenberg, *J. Am. Chem. Soc*., 2004, **126**, 16841–16849; (f) K. M.-C. Wong, N. Zhu and V. W.-W. Yam. *Chem. Commun*., 2006, 3441–3443.

5. Electric conductive properties of organized structures

Field-Induced Time-Resolved Microwave Conductivity (FI-TRMC) Measurement. FI-TRMC measurements were performed by using metal-insulator-semiconductor (MIS) devices prepared as follows. A quartz substrate (4.9 mm × 50 mm) was treated by UV–O_3 prior to use. For fabrication of the gate electrode, Ti (5 nm) and then Au (20 nm) were deposited on the substrate through a shadow mask in a vacuum deposition system. The area of the gate electrode was 3 mm × 6 mm. The substrate was then set in a vacuum deposition system equipped with an RF-sputtering gun under dry Ar gas at r.t. The SiO_2 gate insulator was deposited by RF-sputtering at 100 W onto the Au gate electrode through a shadow mask under an Ar gas flow at 1.1 Pa. The thickness was approximately 880 nm. A PMMA dielectric layer was spin-coated onto the substrate at 250 nm with 3 wt% PMMA in a toluene solution and annealed at 100 °C under air. An organic semiconductor layer **1b** or **1b**·Cl^--**2b**$^+$ in THF was spin-coated on that substrate. After the deposition of **1b** or **1b**·Cl^--**2b**$^+$, a 20 nm thick Au layer was deposited through a shadow mask to fabricate a source electrode.

FI-TRMC measurements were performed with a microwave circuit using microwaves under ambient atmosphere at r.t. The detailed principle was described in the previous report.[S17] The microwave frequency was adjusted using a signal generator (Rohde Schwarz, SMF 100A), and was about 9.0 GHz. After the MIS device was set in the microwave cavity, the change in the reflected microwave power before and after application of a pulse gate bias voltage V_g (50 ms pulse), was measured using a multifunction generator (Wave Factory, WF 1973). The response of the reflected microwave power, ΔP_R, due to accumulated charge carriers at the interface, and the current injected into the semiconductor–insulator interface, I, were measured using a digital phosphor oscilloscope (Tektronix, TDS 3052B) at each V_g value. The saturated ΔP_R value was converted into $\Delta N\mu$ by the equation below.

$$\Delta P_R = K(\Delta N\mu)$$

where K is an experimental parameter as determined in the previous report.[S17] On the other hand, ΔN was calculated by the measured current profile $I(t)$.

$$\Delta N = \frac{1}{e}\int I(t)\,dt$$

Then, a ΔN–$\Delta N\mu$ plot was drawn by using the above $\Delta N\mu$ and ΔN values at each V_g, affording μ values that correspond to the slope of the ΔN–$\Delta N\mu$ plot.

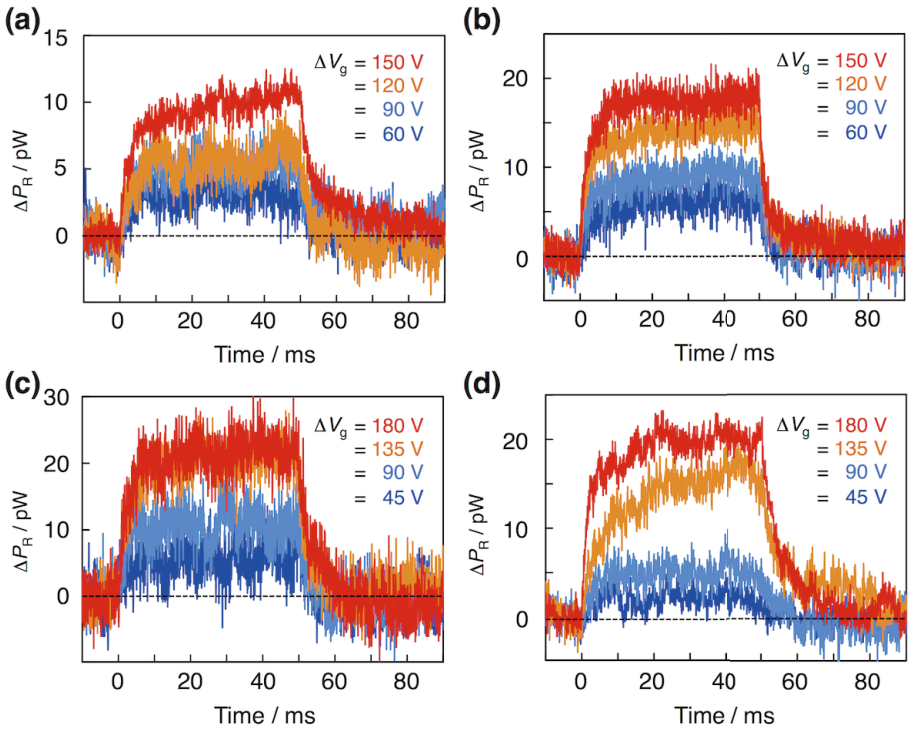

Supporting Figure 13 FI-TRMC profiles ($\Delta P_R(t)$) of (a) **1b** for hole, (b) **1b** for electron, (c) **1b**·Cl^--**2b**$^+$ for hole, and (d) **1b**·Cl^--**2b**$^+$ for electron. ΔV_g indicates the applied gate bias voltage.

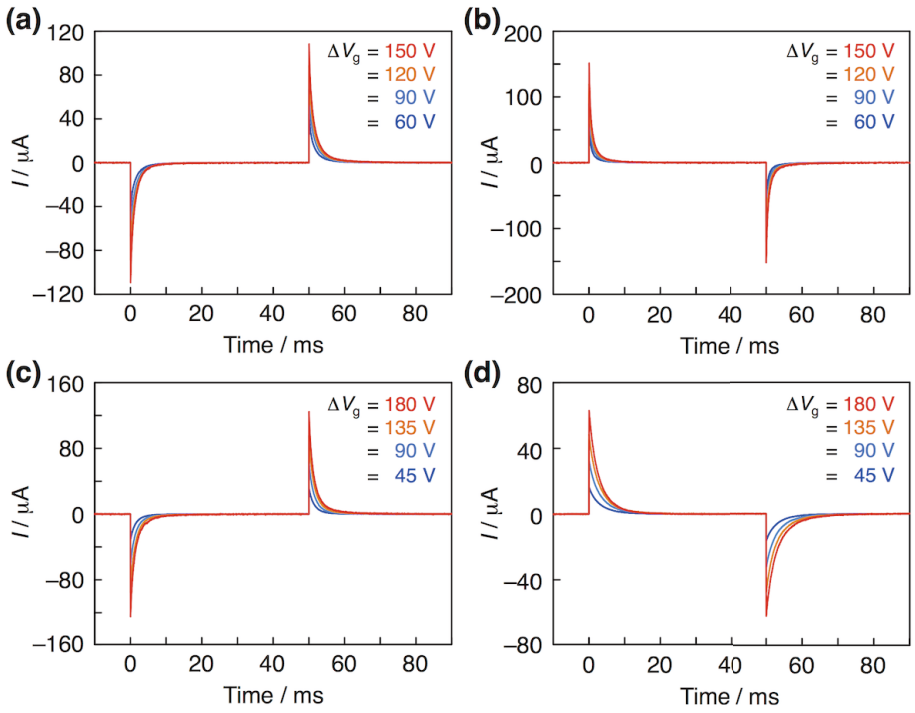

Supporting Figure 14 Current profiles ($I(t)$) of (a) **1b** for hole, (b) **1b** for electron, (c) **1b**·Cl$^-$-**2b**$^+$ for hole, and (d) **1b**·Cl$^-$-**2b**$^+$ for electron. ΔV_g indicates the applied gate bias voltage.

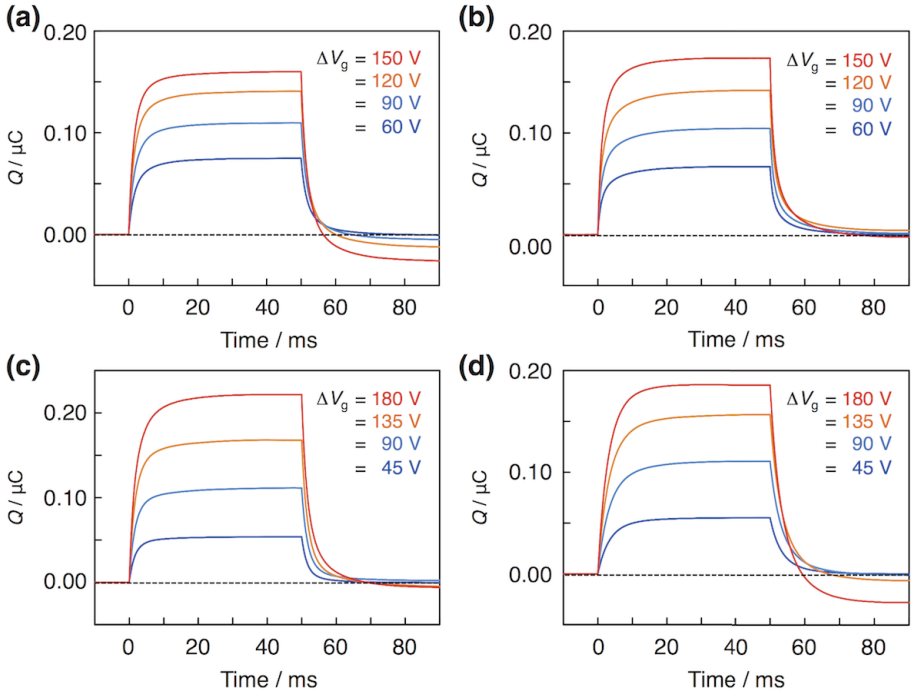

Supporting Figure 15 Injected charge amount profiles calculated from $I(t)$ of (a) **1b** for hole, (b) **1b** for electron, (c) **1b**·Cl$^-$-**2b**$^+$ for hole, and (d) **1b**·Cl$^-$-**2b**$^+$ for electron. ΔV_g indicates the applied gate bias voltage. The change of baseline before and after the gate bias application was due to the leak current. The ΔN value was determined considering the leak current.

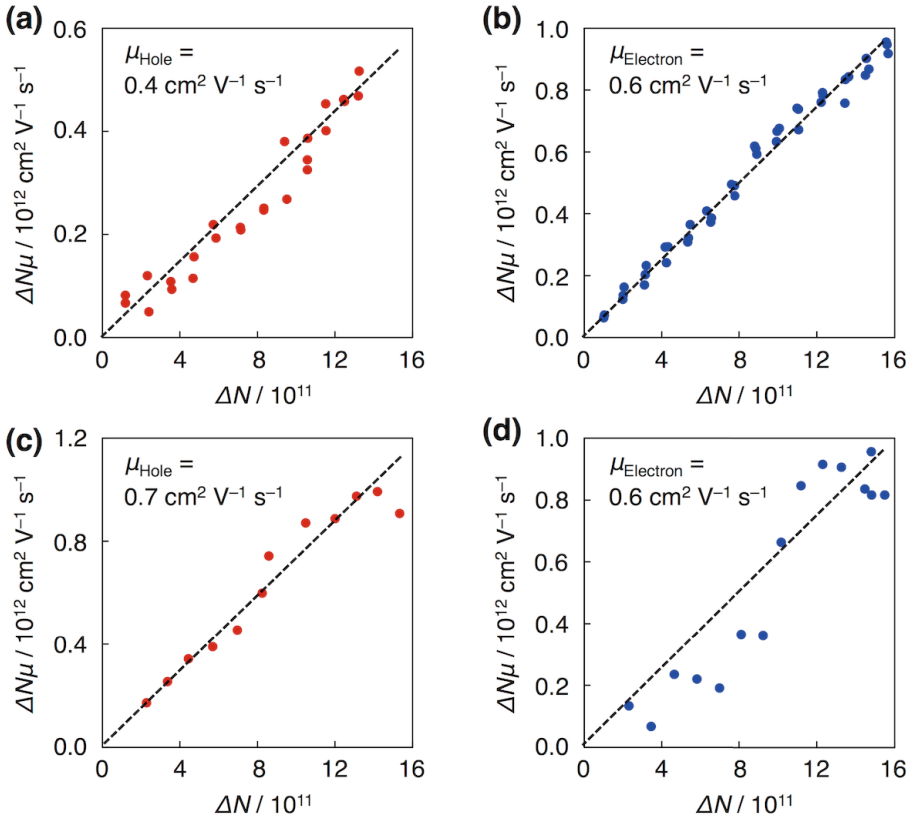

Supporting Figure 16 Δ*N*–Δ*Nμ* plots of (a) **1b** for hole, (b) **1b** for electron, (c) **1b**·Cl⁻-**2b**$^{+}$ for hole, and (d) **1b**·Cl⁻-**2b**$^{+}$ for electron.

[S17] Y. Honsho, T. Miyakai, T. Sakurai, A. Saeki and S. Seki, *Sci. Rep.*, 2013, **3**, 3182.